GRADIVA

Volume 65 | Issue 02 | February 2026
DOI: 10.5281/zenodo.18491366

# Development of a Gesture Controlled Solar Powered Industrial-Based Bladeless Fan from Locally Sourced Waste Materials

Onah, J. N. [1]*, Nwamuo, C. U[2], Akitti, C. O[3] & Ojinnaka, N. C[4]

1,3,4.Department of Electrical and Electronics Engineering, Federal University of Petroleum Resources, Effurun, Delta State, Nigeria.
2.Science Department, Watling Academy Milton Keynes, England, United Kingdom.
*Corresponding Author Email: onah.jonas@fupre.edu.ng

## Abstract

This study presents a pioneering approach to developing gesture controlled industrial-based bladeless fan powered by solar energy, utilizing recycled plastic materials to promote sustainability and cutting-edge technology. A range of carefully selected components, including a microcontroller, ultrasonic sensors, relays, axial flow fan, PVC pipe, and photovoltaic panel, were integrated to create an efficient and reliable system. The materials were chosen for their durability and ability to withstand industrial use, while optimizing fan performance and minimizing energy consumption. The manufacturing process ensures a scalable and cost-effective approach, making it an attractive solution for industrial applications. The system's design incorporates advanced features, such as energy management, obstacle detection, and safe control of high-voltage devices. The microcontroller executes code to control system functions, interacting with sensors and managing battery charge levels. The ultrasonic sensors enable accurate distance measurement and obstacle detection, while the relays provide safe and efficient control of high-voltage devices. The axial flow fan, housed in a lightweight and corrosion-resistant PVC pipe, delivers efficient cooling performance. The system's energy efficiency is achieved through optimizing energy storage and usage, reducing waste and environmental impact. The incorporation of durable components and design features ensures long-term performance and reliability. This study demonstrates a comprehensive approach to developing a sustainable and efficient solar-powered fan system, showcasing the potential for innovative and eco-friendly solutions in industrial applications. By harnessing solar energy and utilizing recycled materials, this study contributes to a more sustainable future.

**Keywords:** *Recycled Plastics, Microcontroller, Ultrasonic Sensors, Relays, Axial Flow Fan, PVC Pipe, and Photovoltaic Panel.*

## 1. INTRODUCTION

Bladeless fan technology represents a significant advancement in airflow generation mechanisms, distinguished primarily by the absence of visible rotating blades, (Determination of Optimum Outlet Slit Thickness and Outlet Angle for the Bladeless Fan Using CFD, 2022).Unlike traditional fans that rely on exposed blades to push air, bladeless fans operate on the principle of air amplification, whereby ambient air is drawn in and accelerated through an annular aperture, creating a smooth and continuous stream of air, (Aslam et al., 2021).The merits of this technology extend notably beyond safety and noise reduction, bladeless fan technology demonstrated energy efficiency benefits due to optimized airflow dynamics that minimize power consumption while maintaining high airflow volumes, (Parlak, 2023).

Moreover, the design promotes ease of maintenance since the absence of external blades reduces debris accumulation and simplifies cleaning. This design marks a departure from the

Volume 65 | Issue 02 | February 2026
DOI: 10.5281/zenodo.18491366

conventional perception of fans, delivering a more ergonomic and aesthetically appealing cooling solution, Hossain et al., 2022). Gesture control technology is increasingly recognized for its potential to revolutionize human-machine interaction by facilitating hands-free and intuitive device operation. In industrial contexts, where workers often engage in manual tasks requiring both hands or wear protective gear hindering manual control interfaces, gesture control provides a significant ergonomic advantage. This technology enables operators to manipulate fan functions—such as power on/off, speed adjustments, and directional control—through simple, natural movements, thereby enhancing operational convenience and safety, (Reddy et al., 2022).

The fundamental advantage of gesture-based control lies in its ability to interpret human motions as commands without the need for physical contact or conventional input devices. This results in reduced contamination risk in sensitive environments, such as clean rooms or food processing facilities, while also accommodating operators with physical disabilities who may find traditional controls challenging. Furthermore, integration of gesture recognition within the Internet of Things (IoT) framework allows for smart industrial appliances capable of remote and automated responses, improving system adaptability and responsiveness, (A et al., 2021).

Modern gesture control systems typically employ a combination of sensors, cameras, and infrared technology to capture and interpret motion data, coupled with advanced algorithms for gesture recognition and command execution. In industrial fans, these technologies can translate complex user inputs into precise control signals, enhancing user experience and operational efficiency. Although, recent studies by (Suraj *et al.*, 2026, Onah et al., 2025) have shown the endless possibilities of artificial intelligence techniques as applied for prediction, the merging of IoT with gesture control not only streamlines control mechanisms but also opens possibilities for predictive maintenance, remote monitoring, and integration with broader industrial automation systems, (Bansal, 2023)

These fans often incorporate energy-saving motor technologies, such as brushless DC motors, optimized for performance under solar power supply constraints. The shift towards solar-powered industrial fans exemplifies the fusion of renewable energy technologies with industrial process optimization, underscoring the relevance of such systems in achieving environmental and economic sustainability objectives Lucky and Ajayi (2023), conducted further research on the design and construction of a solar-powered bladeless fan while using the Switch Mode Power Supply owing to its light weight.

(Bao et al., 2024) primarily investigate the development of functional materials derived from industrial solid wastes for the removal of various gaseous pollutants. (Barbosa et al., 2022), detail the development of novel polymer composites, focusing on an industrial ecology approach by utilizing waste materials from industries located in close proximity. (Karaki et al., 2024), employ Additive Manufacturing (AM) as a key enabler to create Polyethylene (PE)-based composites from industrial waste, focusing on the repurposing of materials to promote environmental sustainability and enhance recycling capacity. (Ni & Friedman, 2024), highlight the challenges of transforming trash and proposed solutions for their effective utilization, particularly in biomanufacturing. In the work done by (Choi et al., 2014), the research motivation is driven by the increasing need for eco-friendly product designs to address global challenges such as global warming, resource depletion, and rising energy costs. While Life Cycle Assessment (LCA) is commonly used to measure environmental impact, an eco-friendly product must also consider performance and usability to be competitive in the market. (Alzhanova et al., 2022) focus on the development of environmentally friendly construction

Volume 65 | Issue 02 | February 2026
DOI: 10.5281/zenodo.18491366

materials by utilizing industrial waste, addressing the significant environmental impact of accumulated industrial waste**.** (Hossain et al., 2022) have the primary goal of designing and developing a bladeless air conditioning fan capable of providing cool air to alleviate summer heat. The Key design considerations included eliminating visible blades and minimizing noise during operation.

The developed bladeless air conditioner fan is presented as superior to typical coolers in several aspects, including cost-effectiveness, aesthetic style, compact size, and shape. Conclusively, the paper describes the design and development of an innovative bladeless air conditioning fan that combines Peltier cooling with a blower mechanism, aiming for quiet operation and a compact, stylish form factor. (Bai'en & Heyu, 2019) did not address gesture control technology integration with solar power for optimizing energy efficiency in industrial-based bladeless fans. The focus on a solar-powered fan dynamic control system that utilizes solar energy for fan operation and temperature reduction.

The paper written by (Li et al., 2024) presents Solar-Sense, a self-powered gesture recognition system utilizing solar cells, which can be adapted for controlling industrial bladeless fans. This integration enhances energy efficiency by harnessing solar energy for gesture control, promoting sustainable human-computer interaction in industrial settings., (Torres et al., 2024) emphasize gesture recognition's role in enhancing AR applications for industrial equipment, by promoting intuitive interactions and reducing contamination risks. It also highlights the potential for improved safety and efficiency in operations, aligning with the benefits of IoT integration.

## 2. METHODOLOGY

### 2.1 Materials and Methods

The Arduino and ATmega328P microcontroller are used for the design. To ensure effective energy management, protection, and easy control in the solar-powered system, this project incorporates carefully selected components optimized for energy storage performance. The are primary materials chosen, each meeting the study's standards for durability, efficiency, and precise control.

### 2.2 Operating principle

The microcontroller exploited is the Uno R3 that comprises the 14 digital input/output pins, 6 analog input pins, a USB connection for programming and power, a power jack, and a reset button. The Arduino Uno R3 houses the code for the system on its onboard memory. When programming the board, the code is written in the Arduino IDE and then uploaded via USB. The microcontroller executes this code to control the system's functions, such as interacting with sensors, managing the battery charge level, and performing tasks as specified by the program.

Ultrasonic distance sensors are commonly used in various applications, including obstacle detection, distance measurement, and proximity sensing. It works by emitting ultrasonic sound waves and detecting the reflected signal from objects within its range. The ultrasonic sensor being used is the HC-SR04. When an object enters its detection range (2 cm to 400 cm, typically narrowed to a specific range such as 3 cm to 30 cm for this application), the sensor calculates the distance and sends a signal to the microcontroller. This signal is processed to trigger various actions, such as activating motors, LEDs, and the buzzer.

Volume 65 | Issue 02 | February 2026
DOI: 10.5281/zenodo.18491366

In this context, the relay functions as an electrically operated switch that enables a low-voltage control circuit, such as an Arduino or microcontroller, to control higher-voltage devices or components, including the battery and photovoltaic (PV) supply. When the relay closes its switch, it permits current to flow through the battery without requiring the microcontroller to directly handle the high voltage. This setup allows the low-power control system to safely manage the high voltage. The brushless DC fan stands out as a powerful and efficient cooling solution for a wide range of electronic devices and projects. Operating at 12 volts, this fan delivers exceptional airflow, effectively maintaining stable temperatures and preventing overheating. Its advanced brushless design guarantees long-lasting performance, significantly reduces noise and requires minimal maintenance. The specific speed of fan or blower is given by (Srinivasan, 2019),

$$n_{sp} = \frac{n_p\sqrt{Q_p}}{(\Delta P_p)^{3/4}} = n_{sm} = \frac{n_m\sqrt{Q_m}}{(\Delta P_m)^{3/4}} \quad (1)$$

from which the speed of rotation of the prototype $n_{sp}$ could be determined.

From model analysis, we get

$$\frac{Q_p}{Q_m} = x^3 \frac{n_p}{n_m} \quad (2)$$

$where\ x = \frac{D_p}{D_m}$ is the scale effect i.e., the diameter ration between prototype and model. Also from model analysis, we get

$$\frac{H_p}{H_m} = x_1^2 \frac{n_p^2}{n_m^2}\ or\ \sqrt{\frac{H_p}{H_m}} = x\frac{n_p}{n_m} \quad (3)$$

$from\ which, we\ get$

$$\frac{Q_p}{Q_m} = x_1^2\sqrt{\frac{H_p}{H_m}}. \quad (4)$$

$$Therefore\ x_1 = \sqrt{\frac{Q_p}{Q_m}\sqrt{\frac{H_p}{H_m}}} \quad (5)$$

where $H = \frac{\Delta p}{\gamma}$. Since $D_p = xD_m$ , all other dimensions can be determined, from the diameter ratio. All references for the determination of main parameters are referred with respect to $\sqrt{2gH}$. Thus outlet peripheral velocity is referred as

$$u_2 = \sqrt{\frac{1}{\Psi}} * \sqrt{2gH}\ H_2^2 = \frac{1}{\Psi} * 2gH\Psi = \frac{H}{(\frac{U^2}{2g})} \quad (6)$$

where $\Psi$ is the non dimensional pressure coefficient. The ration of dynamic pressure $'\Delta p'$ developed, with respect to the outlet peripheral velocity $'\rho u_2^2/2'$ is called pressure coefficient '$\Psi$'. It is a non-dimensional unit

$$\Psi = \frac{2gH}{u_2^2} = \frac{2g\left(\frac{\Delta p}{\gamma}\right)}{u_2^2} = \frac{2\Delta p}{\rho u_2^2} = \frac{\Delta p}{\left(\frac{pu_2^2}{2}\right)} = \frac{2gH}{u_2^2} = \frac{2g\left(\frac{\Delta p}{\gamma}\right)}{u_2^2} = \frac{2\Delta p}{pu_2^2} = \frac{\Delta p}{\left(\frac{\rho u_2^2}{2}\right)} \quad (7)$$

Volume 65 | Issue 02 | February 2026
DOI: 10.5281/zenodo.18491366

Since

$$\Delta p_{th\infty} = \rho u_2 C_{u2th\infty\partial\partial} = \Psi_{th\infty}\left(\frac{\rho u_2^2}{2}\right) \quad (8)$$

$$\Delta p_{th} = \rho u_2 C_{u2th} = \Psi_{th}\left(\frac{\rho u_2^2}{2}\right) \quad (9)$$

$$\Delta p = \rho u_2 C_{u2th\eta hy} = \Psi(\frac{\rho u_2^2}{2}) \quad (10)$$

$$\Psi_{th\infty} = 2\frac{C_{u2th\infty}}{u_2} \quad (11)$$

$$\Psi_{th} = 2\frac{C_{u2th}}{u_2} \quad (12)$$

$$\Psi = 2\eta_{hy}\frac{C_{u2th}}{u_2} \quad (13)$$

Flow coefficient $'\phi'$ is defined as the ratio of flow velocity at outlet $'C_{m2}'$ to outlet peripheral velocity $'u_2'$.

$$\varphi = \frac{C_{m2}}{u_2} \quad (14)$$

it can be easily seen that $n_s = 3.65n_q$ and

$$n_s = 3.65n\frac{\sqrt{Q}}{H^{3/4}} \quad (15)$$

However, at a later stage, the specific speed was modified and specified as Speed coefficients $'\sigma'$ and in recent times, Diameter coefficient $'\delta'$, was also introduced for fans.

Comparing a model fan, having outside diameter $D_2$, and a pressure increase of $\Delta p$, Taking $C_2$ as the outlet velocity, the total pressure increase will be

$$\Delta p = \left(\frac{\rho}{2}\right)C'^2_2 = \Psi\left(\frac{\rho}{2}\right)u_2^2.\ So, C'^2_2 = u_2\sqrt{\Psi}\,. \quad (16)$$

Diameter $D'_2$ is calculated as

$$Q = \varphi u_2 A = C'_2 A' or\ A' = \frac{A\varphi u_2}{C'} = A\varphi/\sqrt{\Psi} \quad (17)$$

When $\varphi = 1\ and\ \Psi = 1$, we get, the peripheral velocity $u'_2$, we get $\Delta p = 1(\frac{\rho}{2})u'^2_2$ and $Q = 1u'_2\ A' = C'A'$. Hence, $u'_2 = C'$ i.e., outside diameter $D'_2$ of the geometrical impeller is identical with the diameter of the outlet of the model fan.

From

$$(A'A) = (\varphi/\sqrt{\Psi}) \quad (18)$$

Volume 65 | Issue 02 | February 2026
DOI: 10.5281/zenodo.18491366

we get $(\frac{D'_2}{D_2})^2 = \frac{\varphi}{\sqrt{\Psi}}$ or the diameter coefficient $\delta = \left(\frac{D_2}{D'_2}\right) = \frac{\Psi^{1/4}}{\varphi^{1/2}}$ (19)

For the speed $n'$, we get

$$u_2 = \left(\frac{\pi D_2 n}{60}\right) u'_2 = \left(\frac{\pi D'_2 n'}{60}\right) = C'_2 C' = u_2\sqrt{\Psi}\, D'_2\, n' = \sqrt{\Psi} D_2 n. \quad (20)$$

So the speed coefficient $\sigma = \frac{n}{n'} = \left(\frac{D'_2}{D_2}\right)\frac{1}{\sqrt{\Psi}} = \frac{\Psi^{1/2}}{\Psi^{3/4}}$ (21)

Also, $\Psi = \frac{1}{\sigma^2\delta^2}$ $and$ $\varphi = \frac{1}{\sigma\delta^3}$ (22)

Speed coefficient is used for axial flow fans. It indicates how many times greater the number of revolutions of an impeller in relation to the number of revolutions of a model impeller having $\psi = 1$ $and$ $\phi = 1$.

The diameter coefficient will be less than 1 if $\sqrt{\Psi} = \varphi$. Such a case arises in high-speed axial flow impellers

$$\sigma = \frac{2\sqrt{\pi}}{(2g)^{3/4}}\frac{n\sqrt{Q}}{60\ H^{3/4}} = \frac{1}{158}\frac{n\sqrt{Q}}{H^{3/4}} \quad (23)$$

$$= \frac{1}{158} n_q = \frac{1}{576}\, n_s \quad (24)$$

$$\sigma_1 = \frac{1}{28.5}\frac{n\sqrt{Q}}{(\Delta p/p)^{3/4}} \quad (25)$$

$$\delta = \sqrt[4]{\frac{2gH}{C_m^2}} = \sqrt{\frac{\pi D^2}{4}}\,\frac{\sqrt[4]{2gH}}{\sqrt{Q}}$$

$$= 1.866 D \frac{\sqrt[4]{H}}{\sqrt{D}} \quad (26)$$

For the design, the throttling coefficient and the coefficient of performance are given as

Throttling coefficient $\tau = \frac{\varphi^2}{\Psi}$ (27)

Coefficient of performance $\lambda = \frac{\varphi\Psi}{\eta}$ (28)

The block diagram of the system is given as shown in Figure 1.

The final system setup uses a 50W solar panel and a 15V/5A power adapter as the power source to charge the lithium battery pack via a charging circuit. A charging circuit has been designed that would delicately control the delicate process of charging the lithium cells in a manner safe to their limits of voltage and current. Then, the power from the battery pack leads to the Arduino Uno through a 7805-voltage regulator, reducing to a steady 5V for the microcontroller.

The Arduino monitors battery voltage through resistive voltage dividers to avoid overcharging or deep discharging. It also sends signals to the fan speed control module where the speed is adjusted by changes in the user's detected gestures via ultrasonic sensor. This setup enables efficient and responsive user-preference-based fan control.

Volume 65 | Issue 02 | February 2026
DOI: 10.5281/zenodo.18491366

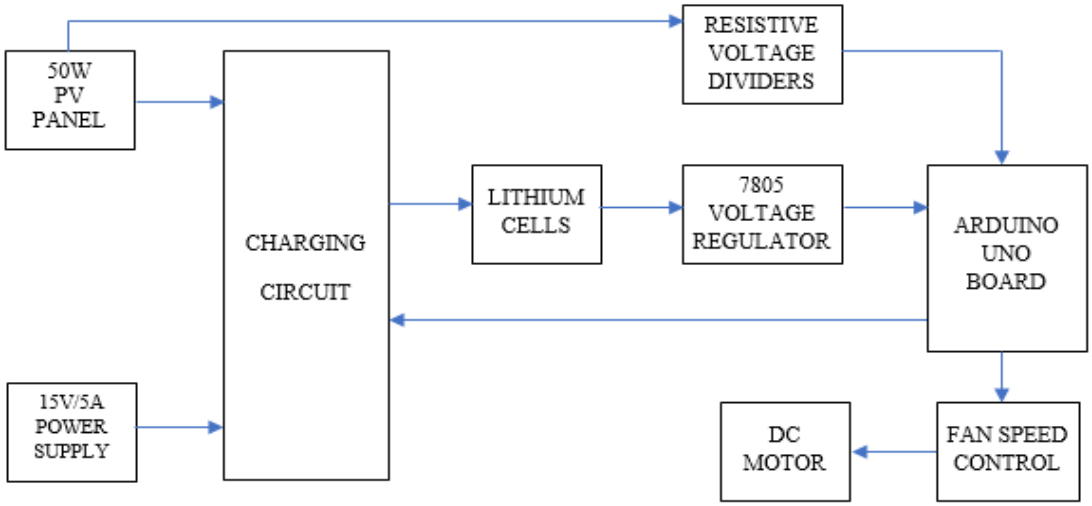


**Figure 1: Complete Functional Block diagram**

## 3.3 Mode of Operation of the Bladeless Fan

### 3.3.1 System Circuit Diagram

Figure 2 shows the simulated circuit design of the system, encompassing both the power and control circuits. The circuit was simulated using Proteus software to verify its functionality.

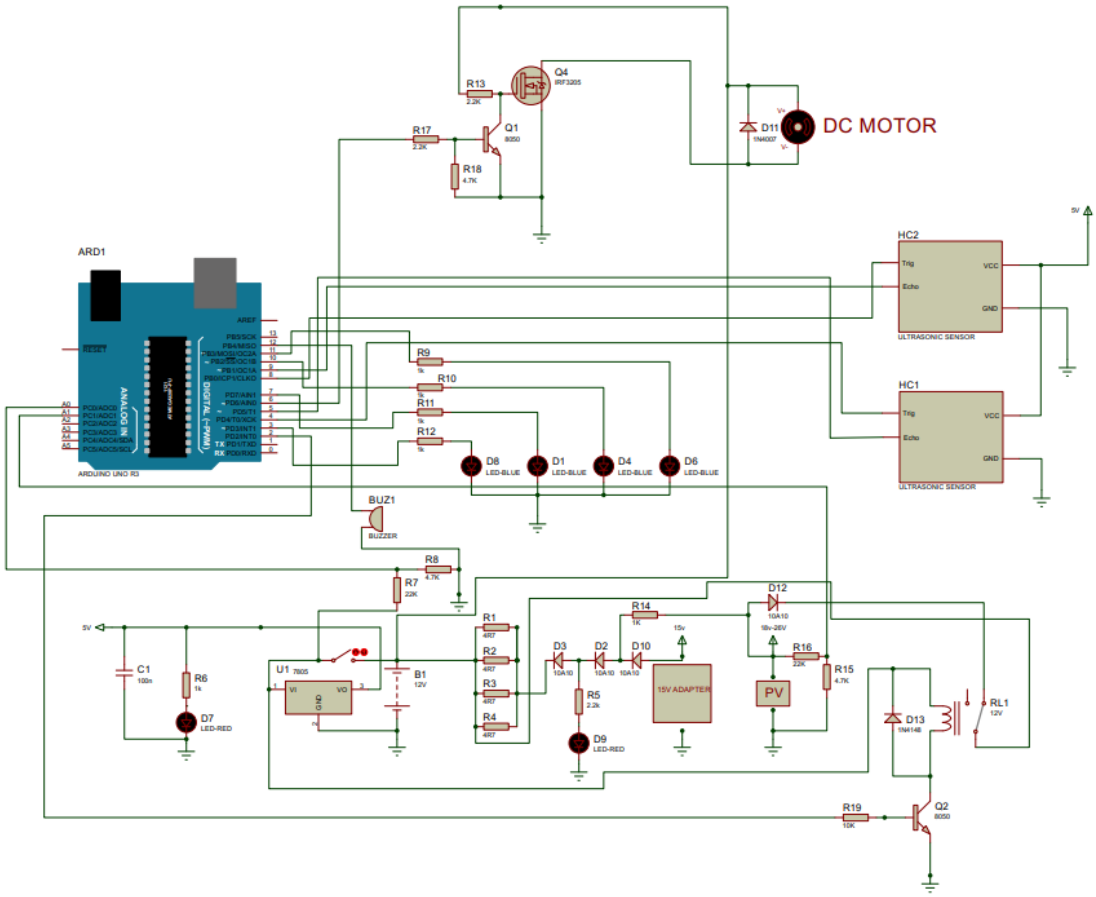


**Figure 2: Simulation of the circuit**

Volume 65 | Issue 02 | February 2026
DOI: 10.5281/zenodo.18491366

The Arduino Uno R3 uses the ATmega328P microcontroller, which has 28 pins, 8 KB SRAM, and 32 KB ROM. It controls the fan speed, monitors the battery voltage, and checks the solar panel's input during charging. The Pins in use are A0 (battery voltage monitoring), A1 (solar panel voltage monitoring), and other pins (A12, A9, A8, A7, A6, A5, A4, A3, and A2) for various inputs and outputs. On this board, there are two pin types; analog pins (A0, A1) which measure voltage using a voltage divider to scale down higher voltages and digital pins which can be configured for input or output based on the code. The speed level indicator is made up of 220 Ω resistors and blue LEDs (D6, D4, D1, and D8) that light up to show the current fan speed. At the lowest speed, only D8 is on, while the rest stay off. As the speed increases, D1 turns on alongside D8. At the next level, D8, D1, and D4 are lit, and at maximum speed, all four LEDs (D8, D1, D4, and D6) light up together. Each LED is controlled by a signal from the Arduino: pin 9 controls D6 through resistor R9, pin 8 controls D4 through R10, pin 7 controls D1 through R11, and pin 6 controls D8 through R12. The resistors limit the current to protect the LEDs, ensuring they work properly without getting damaged. The buzzer is connected to pin 12, and the other end is connected to the ground. It is used to create a beep sound whenever the speed level changes. At the maximum speed, the buzzer gives a double beep sound.

The system needs to monitor the solar panel voltage and the battery voltage to know when the solar panel voltage is available and the level of the battery. The battery's input voltage and the solar panel's input voltage are both monitored. Although the BMS protects the battery from overcharging and discharging below a safe level by disconnecting the load when needed, the monitoring is done on the Arduino Uno R3. Since the Arduino cannot take more than 5V or deliver more than 5V per output, voltage dividers are used to reduce the voltages.

The battery, which is 12V, is connected to the A0 pin of the Arduino through a voltage divider made up of resistors R7 and R6, reducing the voltage to 2V based on the resistor divider rule. The solar panel voltage is also reduced using a voltage divider with resistors R16 and R15, connected to the A1 pin of the Arduino. The Power LED D7 is connected through resistor R6 and serves as the power LED indicator for the circuit. Whenever the circuit is turned on, the LED will light up with a red color to indicate that the system is powered. The charging circuit consists of resistors R1, R2, R3, R4, R14, R5, R19, diodes D3, D2, D10, D12, LED D9, D13, relay RL1, and transistor Q2. The system uses a 15V adapter and a solar panel as the power sources, providing the necessary voltage and current to charge the battery. The components work together to regulate the charging process and ensure the battery is charged properly. Resistors R1, R2, R3, and R4 are connected in parallel to form a total resistance of 1.175 ohms. Diodes D3, D2, and D10 are used to drop the voltage from 15V to 12.9V, since each diode has a 0.7V forward voltage drop, and they are connected in series, adding up to a total drop of 2.1V. The 15V adapter is then connected to the battery through the resistors R1, R2, R3, R4 and diodes D3, D2, and D10. This setup limits the charging current to under 5A, which is the maximum rated current of the adapter.

Resistors R14 and R5 power the LED D9 (Red), indicating whether the adapter or solar panel is connected and providing power. Diode D12 is connected to relay RL1, which in turn is connected to the battery. When the battery is fully charged, the BMS disconnects the battery from the charging source and the load. At this point, the solar panel voltage rises to its open-circuit voltage of 26V, which is too high for the 12V fan circuit. To prevent damage to the circuit, the Arduino detects the high voltage and activates the relay via transistor Q2, switching

Volume 65 | Issue 02 | February 2026
DOI: 10.5281/zenodo.18491366

it from normally closed (NC) to normally open (NO). This disconnects the solar panel from the battery the and the rest of the circuitry, except for D12, R16, R15, R14, R5, and LED D9.

To power up the Arduino and the sensors, a 7805 5V linear regulator is used to step down the voltage from the battery to a stable 5V. A make-and-break switch (SW1) is placed between the regulator's input and the battery, allowing the circuit to be turned ON and OFF. When the switch is closed, the regulator provides the necessary power to the Arduino and sensors; when the switch is open, the circuit is powered off. When the difference between the distance measured by both sensors exceeds a certain amount pre-stated in the program, the Arduino adjusts the speed of the fan in either direction, depending on the difference in distance measured.

The motor driver circuit is made up of transistor Q4, Q1, R13, R17, R18, D11, and C4. Q1, R13, R17, and R18 form an inverter circuit that flips the PWM signals sent from Arduino pin 5. For example, if a PWM signal with a 25% duty cycle is sent, the MOSFET transistor Q4 sees it as 75% duty cycle, and the reverse is also true. The DC motor speed has 4 levels, and the motor completely turns off at the highest PWM duty cycle. This happens because a 100% duty cycle is inverted by the circuit to 0%, which stops the motor. The D11 diode prevents voltage spikes caused by the motor's switching and handles any freewheeling current. C11 helps reduce noise from the motor during switching.

## 4. RESULTS AND DISCUSSION

### 4.1 3D MODEL AND VIEWS

To better visualize the design, a detailed 3D model was created in Revit. The complete 3D model of the bladeless fan, the front view of the fan, the back view of the fan, the side view of the fan, the top, the bottom of the fan, and the complete assembly of bladeless fan are shown in Figures 3 to 11 respectively.

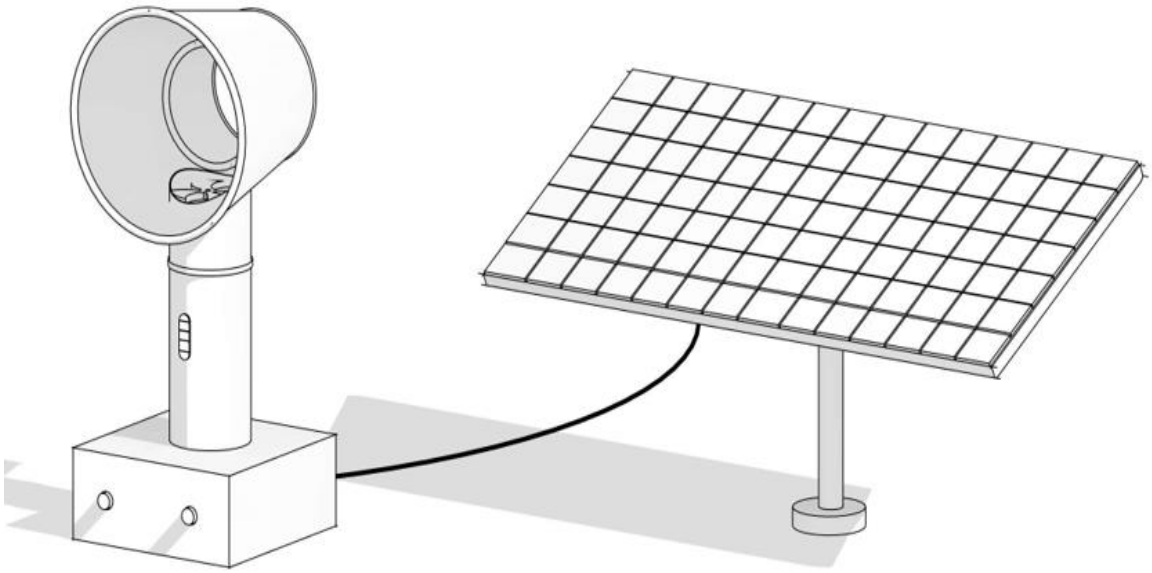

**Figure 3: 3D Model of the Bladeless Fan**

Volume 65 | Issue 02 | February 2026
DOI: 10.5281/zenodo.18491366

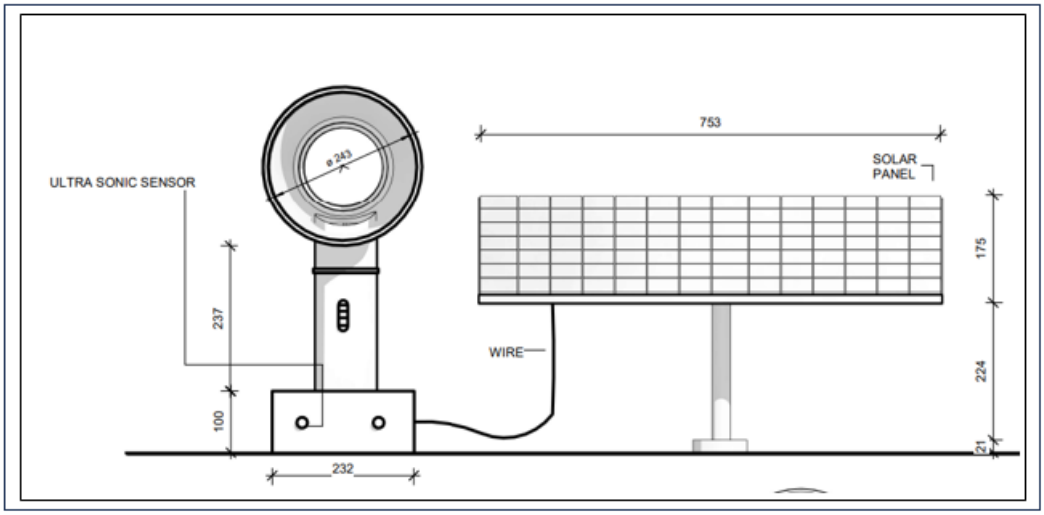


**Figure 4: Front View of the Fan**

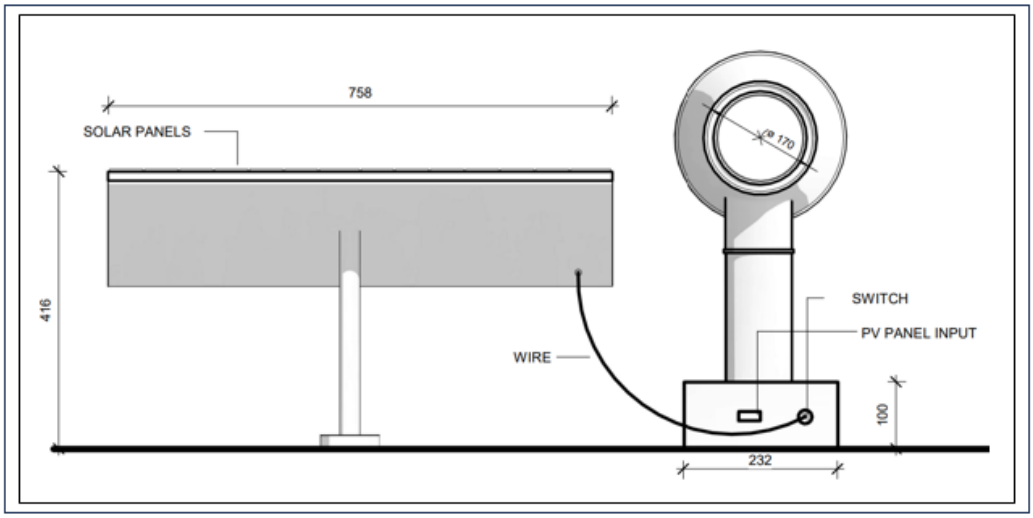


**Figure 5: Back View of the Fan**

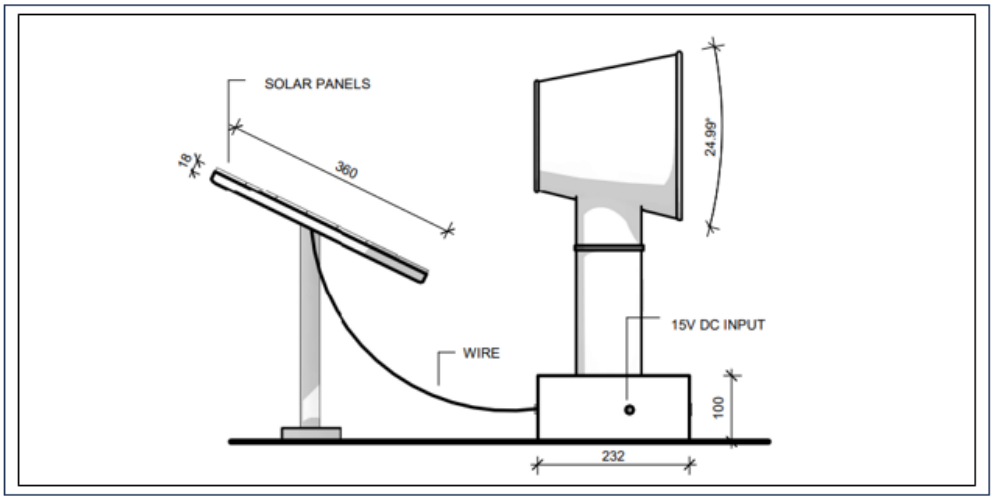


**Figure 6: Side View of the Fan**

Volume 65 | Issue 02 | February 2026
DOI: 10.5281/zenodo.18491366

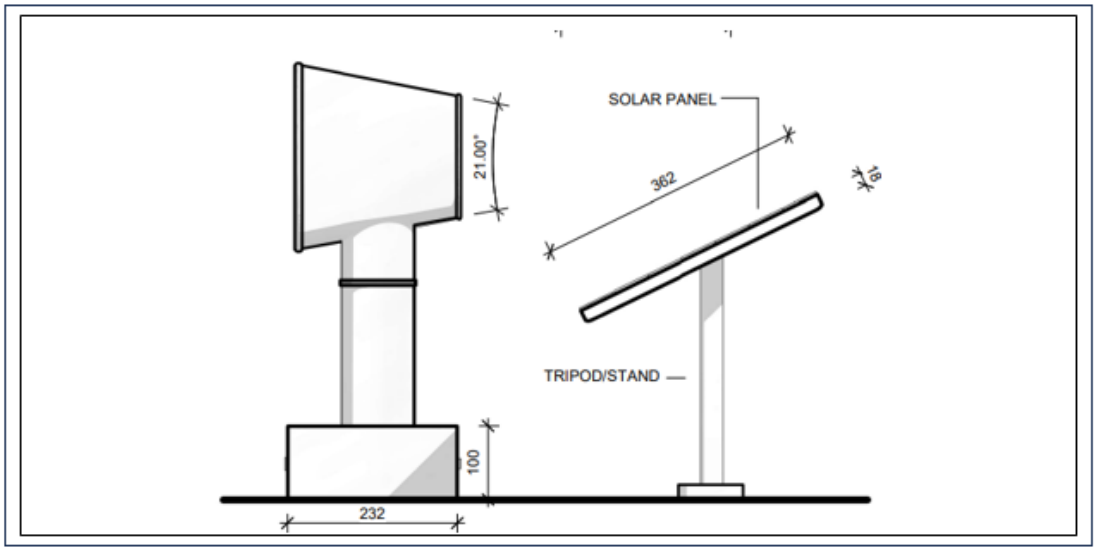


**Figure 7: Side View of the Fan**

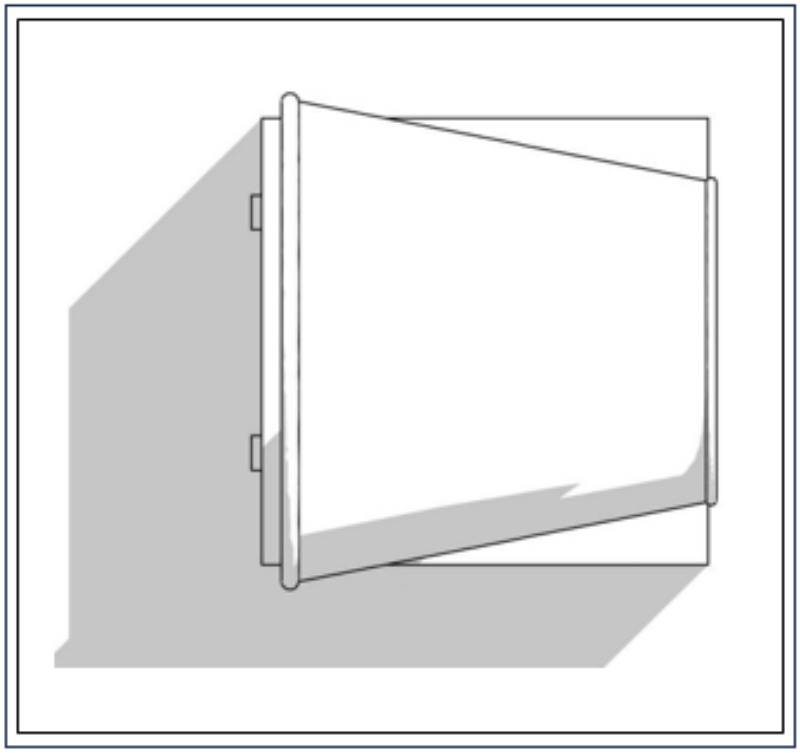

**Figure 8: Top View of the Fan**

The 3D model provides a comprehensive understanding of the bladeless fan's structure. Each view highlights specific aspects critical to its functionality, such as the alignment of the airflow column and the base unit's capacity to house the electronics safely. The ring outlet's aerodynamic design is especially prominent in the top view, emphasizing its role in achieving smooth airflow with minimal energy loss.

Volume 65 | Issue 02 | February 2026
DOI: 10.5281/zenodo.18491366

**Figure 9: Complete assembly of bladeless fan**

### 4.2.1 Aerodynamic Performance Testing

In order to ensure a comprehensive testing of aerodynamic performance of the fan, the noise level, the airflow rate and the velocity profile were ascertained under controlled conditions. Instruments such as acoustic meter was used to obtain the noise level. While anemometer was deployed to assess the airflow volume. The velocity-time graph is as can be observed in Figure 11.

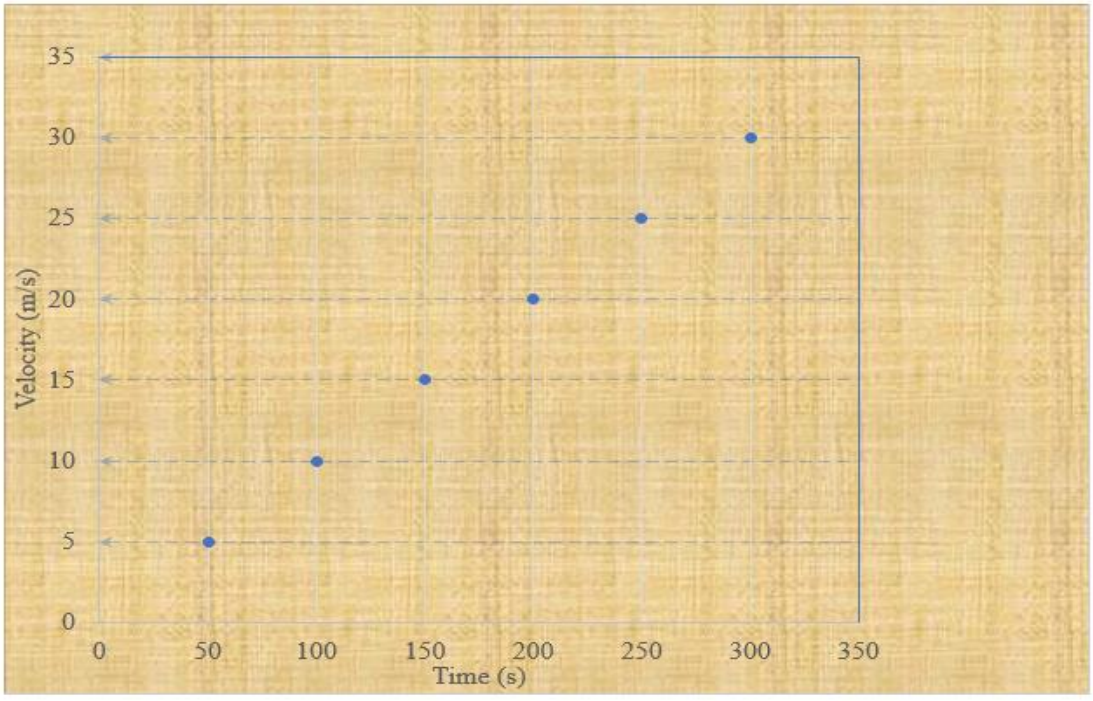


**Figure 10: Velocity time graph**

Volume 65 | Issue 02 | February 2026
DOI: 10.5281/zenodo.18491366

Energy consumption metrics are gathered by monitoring power usage under different solar loads and speed settings, enabling evaluation of efficiency related to the integration of solar power. Comparative testing against traditional bladed fans and non-solar bladeless fans establishes performance baselines, highlighting advantages and areas for improvement. These tests validate the aerodynamic benefits inherent to the bladeless design and assess the impact of utilizing recycled materials on fan performance. Results contribute to refining design parameters and ensuring compliance with industrial standards relating to airflow and noise

### 4.2.2 Solar Power System Efficiency Evaluation

The solar powered bladeless fan comprises a rated 50 W solar panel. Efficiency assessment of the solar power system entails monitoring photovoltaic panel output as can be seen in Figure 11. The operating voltage remains constants until the increase in current due to the fan loading reaches 2.81A. Then, there was sharp decrease in voltage at the knee point of the I-V curve. The maximum power point is estimated to be 50W as can be seen in Figure 11

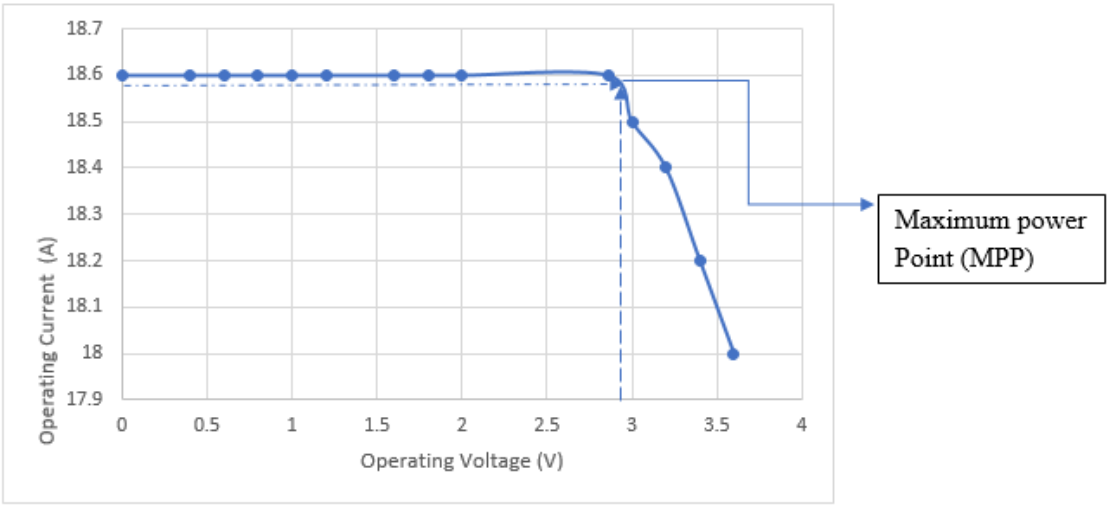


**Figure 11: Maximum power point of the solar panel**

The MPP is estimated to be 50W. Data logging over diurnal and seasonal cycles determines the reliability and consistency of power delivery to the fan under realistic environmental conditions. Factors such as shading, panel orientation, and solar irradiance are analysed to understand their influence on system behaviour. Durability testing with Revit software considers the longevity of components exposed to industrial indoor/outdoor environments and evaluates maintenance requirements over extended operational periods. Such thorough evaluation informs design improvements in solar panel selection and integration strategy, aiming to maximize uptime and minimize downtime due to power shortages or hardware failures.

### 4.2.3 Gesture Control Accuracy and Usability Testing

The gesture control system is subjected to rigorous testing to establish recognition accuracy, latency, and user comfort. Test scenarios simulate industrial lighting conditions and typical operational environments to challenge sensor capabilities and algorithm robustness. User interface testing includes feedback collection from operators to assess intuitiveness of gesture sets, error rates, and system responsiveness. Iterative refinements are made based on this data, improving the ergonomics and reliability of gesture commands. This phase ensures

Volume 65 | Issue 02 | February 2026
DOI: 10.5281/zenodo.18491366

that the developed system meets industrial usability standards, facilitating adoption and demonstrating the practical benefits of advanced control technologies integrated into solar-powered bladeless fans.

### 4.3.1 Energy Consumption and Carbon Footprint Reduction

The combined use of solar power and bladeless fan technology results in considerable energy savings, as the fan consumes less power due to aerodynamic efficiencies and operates on renewable electricity. Quantitative analyses comparing energy consumption of traditional electrically powered fans against the solar-powered, bladeless variant reveal significant reductions in kilowatt-hour usage and associated carbon emissions. Additional environmental benefits arise from reusing waste materials, which diminishes the raw resource extraction footprint and landfill contributions. Lifecycle assessments indicate that the incorporation of recycled fan blade materials notably lowers the carbon footprint of fan production, while operational savings translate into enduring sustainability gains. Such reductions in greenhouse gas emissions align with industrial commitments to environmental stewardship, supporting corporate responsibility goals and regulatory compliance in emissions reduction

### 4.3.2 Cost-Benefit Analysis of Using Local Waste Materials

Economic considerations include lowered raw material procurement costs through utilization of local waste, which circumvents expenses associated with virgin material sourcing and transportation. Processing waste materials also offers local employment opportunities, promoting circular economic growth within communities. Operational savings from solar power usage compound these benefits, reducing electricity bills and vulnerability to energy price fluctuations. Initial investments may be higher due to technology integration costs; however, the return on investment (ROI) often materializes over medium- to long-term operational periods due to decreased energy expenses and material costs. These analyses strongly support the feasibility of scaling up production using waste materials, with positive implications for regional economic resilience and sustainability

### 4.3.3 Market Potential and Scalability

Market analyses forecast increasing demand for energy-efficient and environmentally conscious industrial fans, driven by rising energy costs and tightening sustainability regulations. Solar-powered bladeless fans incorporating recycled materials fit well within these trends, offering a unique value proposition. Scaling production from prototypes to mass manufacturing involves overcoming challenges related to supply chain consistency of waste materials, quality control, and regulatory certifications. However, the sustainability credentials of these fans provide competitive advantages in green markets and industrial sectors prioritizing eco-friendly technologies. Successful integration of advanced features such as gesture control further differentiates these products, expanding their appeal across diverse industrial applications. The synergy of innovations positions this technology for sustainable market growth.

## 5. CONCLUSION

The evaluation indicates that combining gesture control technology with solar-powered, bladeless fan designs is an effective approach to developing next-generation industrial cooling systems. Employing locally sourced waste materials for fan construction demonstrates a viable path to sustainability by reducing resource consumption and waste generation. Empirical and theoretical assessments underscore operational benefits including improved safety, energy

Volume 65 | Issue 02 | February 2026
DOI: 10.5281/zenodo.18491366

efficiency, and ease of use. The integration of advanced control mechanisms enhances accessibility and control precision, establishing a technologically holistic solution for industrial environments. The developed gesture controlled industrial-based bladeless fan is powered by solar energy, which utilizes recycled plastic materials to promote sustainability and cutting-edge technology. The microcontroller executed codes that controlled system functions which interact with sensors and manages the battery charge levels. The axial flow fan, housed in a lightweight and corrosion-resistant PVC pipe, delivers efficient cooling performance. The system's energy efficiency is achieved through optimizing energy storage and usage, reducing waste and environmental impact. The incorporation of durable components and design features ensures long-term performance and reliability. This study demonstrates a comprehensive approach to developing a sustainable and efficient solar-powered fan system, showcasing the potential for innovative and eco-friendly solutions in industrial applications. By harnessing solar energy and utilizing recycled materials, more sustainable future is assured.

**References**

1) A, H., P, H., & Asha, P. (2021). *Gesture based Home appliance control system for Disabled People*. https://doi.org/10.1109/ICESC51422.2021.9532973

2) Alzhanova, G. Z., Aibuldinov, Y. K., Iskakova, Z. B., Khabidolda, S. M., Abdiyussupov, G. G., Omirzak, M. T., Murali, G., & Vatin, N. (2022). Development of Environmentally Clean Construction Materials Using Industrial Waste. *Materials*, *15*(16), 5726. https://doi.org/10.3390/ma15165726

3) Araújo, Í. B. Q. (2024). *A Framework for Real-Time Gestural Recognition and Augmented Reality for Industrial Applications*. https://doi.org/10.3390/s24082407

4) Aslam, H., Arif, M. Z., Ali, M., & Javed, A. (2021). *Design and CFD Analysis of Bladeless Ceiling Fan*. https://doi.org/10.1109/IBCAST51254.2021.9393254

5) Bai'en, H., & Heyu, H. (2019). *Solar powered fan dynamic control system*. https://scispace.com/papers/solar-powered-fan-dynamic-control-system-56vulzvb4x

6) Bao, J., Sun, X., Ning, P., Li, K., Yang, J., Wang, F., Shi, L., & Fan, M. (2024). *Industrial solid wastes to environmental protection materials for removal of gaseous pollutants: A review*. https://doi.org/10.1016/j.gee.2024.01.006

7) Bansal, J. L. (2023). Gesture-based Human-Computer Interaction using Wearable Devices. *International Journal for Research Publication and Seminar*, *14*(4), 141–150. https://doi.org/10.36676/jrps.2023-v14i40

8) Choi, Y., Lee, B. H., & You, H. (2014). *A Case Study of Eco-Design for a Bladeless Fan by Performance, Usability, and Life Cycle Assessments*. https://doi.org/10.62765/kjlca.2014.15.1.143

9) *Determination of Optimum Outlet Slit Thickness and Outlet Angle for the Bladeless Fan Using CFD*. (2022). https://doi.org/10.20944/preprints202211.0459.v1

10) Hossain, M. S., Hossen, M. N., Hossain, M. N., Uddin, N., Mahbub, M., Ahmmed, M. S., & Haque, M. A. (2022). *Ecofriendly Design and Development of Bladeless Air Conditioning Fan*. https://doi.org/10.46254/bd05.20220131

Volume 65 | Issue 02 | February 2026
DOI: 10.5281/zenodo.18491366

11) Karaki, A., Argyros, A., Stratiotou-Efstratiadis, V., Khraisheh, M., Masad, E., & Michailidis, N. (2024). Additive manufacturing of polyethylene-based composites sourced from industrial waste. *CIRP Annals*. https://doi.org/10.1016/j.cirp.2024.03.012

12) Li, J., Xu, Q., Zhu, Q.-C., Xie, Z., Xu, Z., Ge, C., Ruan, L., Fu, H. Y., Liang, X., Ding, W., Gui, W., & Zhang, X.-P. (2024). *Demo: SolarSense: A Self-powered Ubiquitous Gesture Recognition System for Industrial Human-Computer Interaction*. https://doi.org/10.1145/3643832.3661838

13) Onah, J.N, Egbuson, N.E, Obi N.O & Akitti C.O.(2025). Development of a Gas Leakage Detection and Alert System for Enhanced Safety. Gradiva 64 (12), 167-179. DOI: 10.5281/zenodo.18130066

14) Ni, C., & Friedman, D. C. (2024). Transforming trash: strategies to develop waste into a feedstock for a circular bioeconomy. *Biofuels, Bioproducts and Biorefining*. https://doi.org/10.1002/bbb.2586

15) Parlak, Z. (2023). Numerical investigation of aerodynamic performance and noise characteristic of air multiplier bladeless fan. *International Advanced Researches and Engineering Journal*, 13–22. https://doi.org/10.35860/iarej.1148880

16) Reddy, P. R., Katte, P., Soni, P., Agrawal, G., Kundu, S., & Santhi, V. J. (2022). *GestFanz - A Human Machine Interactive Model for Fan Automation*. 59–63. https://doi.org/10.1109/ICICICT54557.2022.9917625

17) Torres, W., Santos, L., Melo, G., Oliveira, A., Nascimento, P., Carvalho, G., Neves, T., Martins, A., & Srinivasan, K. M., 2019. Fans and Blowers. New age international publishers.

18) Suraj. A, Anju, J. N. Onah. (2026). A Data-Driven Framework for Methane Emission Prediction Using Machine Learning Methods *ICCK Transactions on Machine Intelligence* 2(1): 53-64, 2026 | DOI: 10.62762/TMI.2025.782852